Analysis of entrance region flow of Bingham nanofluid in concentric annuli with rotating inner cylinder

Selvam Mullai Venthan[1] ✉, *Isaac Jayakaran Amalraj*[1], *Ponnusamy Senthil Kumar*[2,3]

[1]*Department of Mathematics, SSN College of Engineering, Chennai, Tamilnadu, 603 110, India*
[2]*Department of Chemical Engineering, SSN College of Engineering, Chennai, Tamilnadu, 603 110, India*
[3]*SSN-Centre for Radiation, Environmental Science and Technology (SSN-CREST), SSN College of Engineering, Chennai 603110, India*
✉ *E-mail: selvamullai11@email.com*

Published in Micro & Nano Letters; Received on 17th July 2019; Revised on 4th September 2019; Accepted on 18th September 2019

This work analyses the entrance region flow of Bingham nanofluids in cylindrical concentric annuli. In this discussion, water is used as the base fluid which is embedded with the silver(Ag) and copper(Cu) nanoparticles coalescing with Bingham fluid. The investigation has been carried out by rotating the inner cylinder, while the outer cylinder is assumed to be at rest. A finite-difference analysis is used to obtain the axial, radial, tangential velocity components and the pressure along the radial direction. With the Prandtl's boundary layer assumptions, the continuity and momentum equations are solved iteratively using a finite difference method. Computational results are obtained for various non-Newtonian flow parameters, different volume fraction parameters and geometrical considerations. This work's main interest is to study the development of velocity profiles and pressure drop in the entrance region of the annuli. The present results are compared with the results available in the literature for various particular cases and it is found to be in good agreement.

Nomenclature

m	number of radial increments in the numerical mesh network
p, p_0	pressure and initial pressure, respectively, Pa
P	dimensionless pressure
r, θ, z	cylindrical coordinates
η and ς	dimensionless coordinates in the radial and axial directions, respectively
B	Bingham number
Re, Ta	modified Reynolds number and Taylor number, respectively
$\mathrm{Rt} = \mathrm{Re}^2/\mathrm{Ta}$	ratio of Reynolds number with Taylors number
R	aspect ratio of the annulus, r_1/r_2 (flow region of an annular space)
r_1, r_2	radius of the inner and outer cylinders, respectively
v_z, v_r, v_θ	velocity components in z, r, θ directions, respectively, m/s
v_0	uniform inlet velocity, m/s
k	coefficient of fluidity
U, V, W	dimensionless velocity components
ϕ	volume fraction of the nanofluid
ρ	density of the fluid, $\mathrm{Kg/m^3}$
ρ_{nf}	density of the Bingham nanofluid
μ	apparent viscosity of the model, Kg/m s
μ_{r}	reference viscosity
μ_{nf}	viscosity of the Bingham nanofluid
ω	angular velocity, rad/s
$\Delta\eta$, $\Delta\varsigma$	mesh sizes in the radial and axial directions, respectively.

1. Introduction: Recently, the study of non-Newtonian flow has been a tremendous attraction in fluid dynamics research. In particular, non-Newtonian fluid characterised by a yield value such as Bingham plastics, Casson and Herschel-Bulkley fluids are the special interest of the tribologists. The applications of non-Newtonian fluids are evident in polymer devolatisation and processing, wire and fiber coating, heat exchangers, extrusion process, chemical processing equipment, etc. Many important industrial fluids are non-Newtonian in their characteristics and are referred to as rheological fluids. This includes blood, coal–water or coal–oil slurries, glues, inks, foods, polymer solutions, paints, grease, paste, jelly and many others. In this analysis the non-Newtonian fluid considered here is the Bingham plastic.

On the other hand, nanotechnology has been widely used in many industrial applications. Nanofluids are engineered colloids made up of a base fluid and nanoparticles, i.e. nanofluid is the composite of nano-sized particles, like, copper, silver, gold, carbon nanotubes etc. and the base fluids, like, water, engine oil, glycerin, etc. Choi and Eastman [1] were the first one who gave the idea of utilising composite fluid, namely, nanofluids, they used two different types of nanofluids, copper (copper with water) and silver (silver with water), in their study. The reasons for the use of water-based Ag and Cu are generally regarded as a safe material for humans and animals although it is recognised that this may change in the future with more fundamental research on nano-toxicology.

Further, both experimental and theoretical analyses are carried out with the experimental work on ethylene glycol-based nanofluids containing with spherical TiO_2 nanoparticles and the theoretical analyses on the high shear viscosity, shear-thinning behaviour and temperature dependence by Chen *et al.* [2]. This work aims at a more fundamental understanding of the rheological behaviour of nanofluids and the interpretation of the discrepancy. Hojjat *et al.* [3] investigated experimentally the forced convective heat transfer of three kinds of nanofluids, prepared by dispersing g-Al_2O_3, CuO, and TiO_2 nanoparticles in an aqueous solution of the carboxymethylcellulose. The base fluid and all nanofluids show pseudoplastic rheological behaviour through a uniformly heated circular tube under turbulent flow conditions. Esmaeilnejad *et al.* [4] investigated the advantages of using nanoparticles with particular size in non-Newtonian fluids. They have computed numerically the convection of heat transfer and laminar flow of nanofluids with non-Newtonian base fluid through rectangular microchannels. Hayat *et al.* [5] discussed the boundary layer flow of a Casson fluid due to a stretching cylinder in the presence of nanoparticles and thermal radiation. Here all physical properties are taken as constant for the Casson fluid, except the thermal conductivity.

Usman *et al.* [6] investigated numerically the velocity and thermal slip effects on Casson nanofluid with heat and mass transfer phenomena over an inclined permeable stretching cylinder by using the collocation method.

Even though many research works have been carried out separately in entrance region study as well as about nanofluids by various researchers, the study of entrance region flow using nanofluids has been very rare, therefore we intend to do that work. In this research article, the entrance region flow of a Bingham fluid in the presence of nanofluids has been studied in cylindrical concentric annuli. The focus will be on nanofluids containing Ag and Cu by using water as base fluid, and the theoretical analysis is based on our current understanding of the rheology of Bingham fluid. The problem of entrance region flow of Bingham nanofluid in concentric annuli has been investigated. The analysis has been carried out under the assumption that the inner cylinder is rotating and the outer cylinder is at rest. With Prandtl's boundary layer assumptions and the equations of conservation of mass and momentum are solved using linearised implicit finite difference technique. The system of linear algebraic equations thus obtained has been solved by the Gauss-Jordan method. The present study reports the development of axial, radial, tangential velocity profiles and pressure drop in the entrance region for different values of Bingham fluid characteristics, different volume fraction parameters for Ag–water and Cu–water under various geometrical parameters. The effects of these on the velocity profiles and pressure drop have been discussed.

2. Analysis of the problem: The flow of two different nanofluids are considered namely Ag-nanofluid and Cu-nanofluid and they are coalescing with Bingham fluid and entering into the horizontal rotating concentric circular cylinders, from a large chamber with a uniform velocity v_0 and pressure p_0 initially. The radius of the inner and outer cylinders is r_1 and r_2, respectively. Here ω is the angular velocity for rotating inner cylinder where the outer cylinder is assumed to be at rest. The laminar flow is steady and incompressible, with the physical properties being constants. We consider a cylindrical polar coordinates system (r, θ, z) fixed at the entry section with r and z along the radial and axial direction, respectively. The geometry of the problem is shown in Fig. 1.

The constitutive equation and governing equations for nanofluid with the Bingham fluid are given as from Nadiminti and Kandasamy [7].

$$\tau_{ij} = \left(\mu_{\rm nf} + \frac{\tau_0}{\varepsilon}\right)\varepsilon_{ij} \quad \tau \geq \tau_0$$
$$\text{where} \quad \tau = \sqrt{\frac{1}{2}\tau_{ij}\tau_{ij}} \text{ and } \varepsilon = \sqrt{\frac{1}{2}\varepsilon_{ij}\varepsilon_{ij}} \tag{1}$$

where τ_0 is the yield stress, $\mu_{\rm nf}$ is the viscosity of the Bingham nanofluid. τ_{ij} and ε_{ij} are the stress tensor and the rate-of-strain tensor,

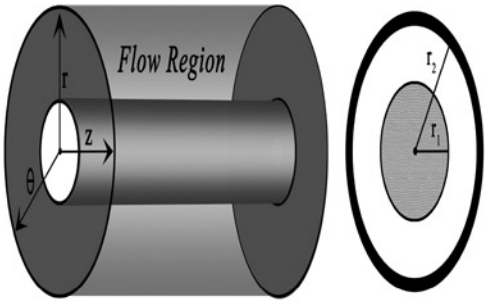

Fig. 1 *Geometry of the concentric coaxial cylinders*

respectively. The flow is governed by the equations

$$\frac{\partial}{\partial r}(rv_r) + \frac{\partial}{\partial z}(rv_z) = 0 \tag{2}$$

$$\frac{v_\theta^2}{r} = \frac{1}{\rho_{\rm nf}}\frac{\partial p}{\partial r} \tag{3}$$

$$v_r\frac{\partial(v_\theta)}{\partial r} + v_z\frac{\partial(v_\theta)}{\partial z} + \frac{vv_\theta}{r} = \frac{1}{\rho_{\rm nf}r^2}\frac{\partial}{\partial r}\left(r^2\left[\tau_0 + kr\frac{\partial}{\partial r}\left(\frac{v_\theta}{r}\right)\right]\right) \tag{4}$$

$$v_r\frac{\partial(v_z)}{\partial r} + v_z\frac{\partial(v_z)}{\partial z} = -\frac{1}{\rho_{\rm nf}}\frac{\partial p}{\partial z} + \frac{1}{\rho_{\rm nf}r}\frac{\partial}{\partial r}\left(r\left[\tau_0 + k\frac{\partial v_z}{\partial r}\right]\right) \tag{5}$$

where v_r, v_θ, v_z are the velocity components in r, θ, z directions, respectively. $\rho_{\rm nf}$ is density of the Bingham nanofluid. For the inner cylinder rotation, the boundary conditions are

$$\begin{aligned} &\text{For } z \geq 0 \text{ and } r = r_1,\ v_r = v_z = 0 \text{ and } v_\theta = \omega r_1 \\ &\text{For } z \geq 0 \text{ and } r = r_2,\ v_r = v_z = 0 \text{ and } v_\theta = 0 \\ &\text{For } z = 0 \text{ and } r_1 < r < r_2,\ v_z = v_0 \\ &p = p_0 \text{ at } z = 0 \end{aligned} \tag{6}$$

Using the boundary conditions, the continuity (2) can be expressed in the following integral form

$$2\int_{r_2}^{r_1} rv_z \mathrm{d}r = \left(r_2^2 - r_1^2\right)v_0 \tag{7}$$

The non-dimensionalisation of the parameters are as follows:

$$\begin{aligned} &\eta = \frac{r}{r_2},\ U = \frac{v_z}{v_0},\ V = \frac{\rho_{\rm nf}v_r r_2}{\mu_{\rm f}},\ W = \frac{v_\theta}{\omega r_1}, \\ &R = \frac{r_1}{r_2},\ P = \frac{p - p_0}{\rho_{\rm nf}v_0^2},\ \zeta = \frac{2v_z(1-R)}{r_2 \mathrm{Re}}, \\ &B = \frac{\tau_0 r_2}{kv_0},\ \mathrm{Re} = \frac{2\rho_{\rm nf}(r_2 - r_1)v_0}{k}, \\ &T_a = \frac{2\omega^2\rho_{\rm nf}^2 r_1^2(r_2 - r_1)^3}{\mu_{\rm f}^2(r_1 + r_2)},\ \text{where } \mu_{\rm f} = k\left(\frac{\omega r_1}{r_2}\right) \\ &\rho_{\rm nf} = (1-\phi)\rho_{\rm f} + \phi\rho_{\rm s},\ \mu_{\rm nf} = \frac{\mu_f}{(1-\phi)^{2.5}} \end{aligned} \tag{8}$$

where η and ς dimensionless coordinates in the radial and axial directions respectively. ϕ is the solid volume fraction of the nanofluid, $\mu_{\rm f}$ is the viscosity of the fluid fraction, $\rho_{\rm f}$ is the reference density of the fluid fraction, $\rho_{\rm s}$ is the reference density of the solid fraction. By introducing the above non-dimensional parameters, the governing (2)–(5) as well as boundary conditions (6), they become

$$\left(\frac{1}{(A_1 * A_2)}\right)\frac{\partial V}{\partial \eta} + \left(\frac{1}{(A_1 * A_2)}\right)\frac{V}{\eta} + \left(\frac{1}{(A_1 * A_2)}\right)\frac{\partial U}{\partial \zeta} = 0 \tag{9}$$

$$\frac{W^2}{\eta} = \frac{\mathrm{Re}^2(1-R)}{2(1+R)Ta}\frac{\partial P}{\partial \eta} \tag{10}$$

$$\begin{aligned} &V\left(\frac{1}{(A_1 * A_2)}\right)\frac{\partial W}{\partial \zeta} + U\frac{\partial W}{\partial \zeta} + \left(\frac{1}{(A_1 * A_2)}\right)\frac{VW}{\eta} \\ &= \left(\frac{1}{(A_1 * A_2)}\right)\frac{\partial^2 W}{\partial \eta^2} + \frac{1}{\eta}\left(\frac{1}{(A_1 * A_2)}\right)\frac{\partial W}{\partial \eta} \\ &- \left(\frac{1}{(A_1 * A_2)}\right)\frac{W}{\eta^2} + \frac{2B}{\eta}\left(\frac{1}{A_2}\right) \end{aligned} \tag{11}$$

doi: 10.1049/mnl.2019.0437

$$V\frac{\partial U}{\partial \eta}\left(\frac{1}{(A_1*A_2)}\right)+U\frac{\partial U}{\partial \zeta}=-\frac{\partial P}{\partial \zeta}+\frac{1}{\eta}\left(\frac{1}{(A_1*A_2)}\right)\frac{\partial U}{\partial \eta}+\left(\frac{1}{(A_1*A_2)}\right)\frac{\partial^2 U}{\partial \eta^2}+\frac{B}{\eta}\left(\frac{1}{A_2}\right) \tag{12}$$

$$2\int_R^1 \eta U d\eta = (1-R^2) \tag{13}$$

where $A_1=((1)/((1-\phi)^{2.5}))$ and $A_2=((1)/((1-\phi)+\phi((\rho_s)/(\rho_f))))$.

Above (9)–(13), and the boundary conditions (6) become

$$\begin{aligned}&\text{For } \varsigma \geq 0 \text{ and } \eta = 1,\ V = U = 0 \text{ and } W = 1\\ &\text{For } \varsigma \geq 0 \text{ and } \eta = R,\ V = U = 0 \text{ and } W = 0\\ &\text{For } \varsigma = 0 \text{ and } R < \eta < 1,\ U = 1\\ &P = 0 \text{ at } \varsigma = 0\end{aligned} \tag{14}$$

3. Numerical solution: The numerical investigation and the scheme of solution can be considered as a roundabout expansion work of Nadiminti and Kandasamy [7]. It has been decided to solve the above system of governing equations, using finite difference method.

The discritised solution space is shown in Fig. 2 in which $\Delta\eta$ and $\Delta\varsigma$ correspond to the grid size along the radial direction and also axial direction, respectively. By assuming appropriate finite-difference definitions, the non-dimensionalised system of (9)–(13) got reduced as

$$V_{(i+1)}^{(n+1)}\left(\frac{1}{(A_1*A_2)}\right)=V_i^{(n+1)}\left(\frac{1}{(A_1*A_2)}\right)\left(\frac{R+i\Delta\eta}{R+(i+1)\Delta\eta}\right)-\frac{4\Delta\eta}{4\Delta\varsigma}\left(\frac{1}{(A_1*A_2)}\right)\left(\frac{2R+(2i+1)\Delta\eta}{R+(i+1)\Delta\eta}\right)*\left(U_{i+1}^{(n+1)}+U_i^{((n+1)}-U_i^{(n+1)}-U_i^{(n)}\right) \tag{15}$$

$$\frac{[W^2]_i^{(n+1)}}{R+i\Delta\eta}=\frac{(1-R)\mathrm{Re}^2}{2Ta(1+R)}\frac{P_i^{(n+1)}-P_{i-1}^{(n+1)}}{\Delta\eta} \tag{16}$$

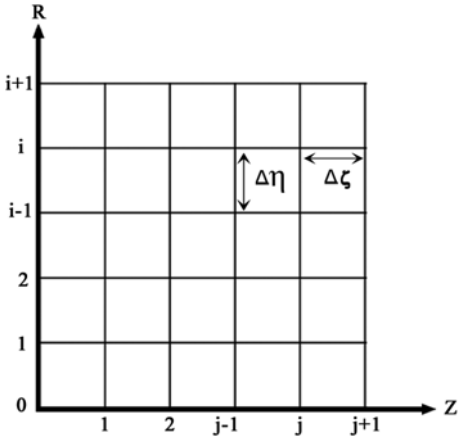

Fig. 2 *Meshwork for the finite difference technique*

$$\begin{aligned}&V_i^{(n)}\left[\frac{W_{i+1}^{(n+1)}+W_{i+1}^{(n)}-W_{i-1}^{(n+1)}-W_{i-1}^{(n)}}{4\Delta\eta}\right]*\left(\frac{1}{(A_1*A_2)}\right)\\ &+U_i^{(n)}\left[\frac{W_i^{(n+1)}-W_i^{(n)}}{\Delta\varsigma}\right]+\left[\frac{V_i^{(n)}W_i^{(n)}}{R+i\Delta\eta}\right]*\left(\frac{1}{(A_1*A_2)}\right)\\ &=\left[\frac{W_{i+1}^{(n+1)}+W_{i+1}^{(n)}-2W_i^{(n+1)}-2W_i^{(n)}}{2(\Delta\eta)^2}\right]*\left(\frac{1}{(A_1*A_2)}\right)\\ &+\left[\frac{W_{i-1}^{(n)}-W_{i-1}^{(n+1)}}{2(\Delta\eta)^2}\right]*\left(\frac{1}{(A_1*A_2)}\right)-\left[\frac{W_i^{(n)}}{(R+i\Delta\eta)^2}\right]*\left(\frac{1}{(A_1*A_2)}\right)\\ &+\left[\frac{W_{i+1}^{(n+1)}+W_{i+1}^{(n)}-W_{i-1}^{(n+1)}-W_{i-1}^{(n)}}{(R+i\Delta\eta)4\Delta\eta}\right]*\left(\frac{1}{(A_1*A_2)}\right)\\ &+\left[\frac{2B}{R+i\Delta\eta}\right]*\left(\frac{1}{A_2}\right)\end{aligned} \tag{17}$$

$$\begin{aligned}&V_i^{(n)}\left[\frac{U_{i+1}^{(n+1)}-U_{i-1}^{(n+1)}}{2\Delta\eta}\right]*\left(\frac{1}{(A_1*A_2)}\right)+U_i^{(n)}\left[\frac{U_i^{(n+1)}-U_i^{(n)}}{\Delta\varsigma}\right]\\ &=-\left[\frac{P_{i+1}^{(n+1)}-P_i^{(n)}}{\Delta\varsigma}\right]+\left[\frac{U_{i+1}^{(n+1)}-U_{i-1}^{(n+1)}}{(R+i\Delta\eta)2\Delta\eta}\right]*\left(\frac{1}{(A_1*A_2)}\right)\\ &\left[\frac{U_{i+1}^{(n+1)}-2U_i^{(n+1)}-U_{i-1}^{(n+1)}}{(\Delta\eta)^2}\right]*\left(\frac{1}{(A_1*A_2)}\right)\\ &+\left[\frac{B}{R+i\Delta\eta}\right]*\left(\frac{1}{A_2}\right)\end{aligned} \tag{18}$$

where $i=0$ at $\eta=R$ and $i=m$ at $\eta=1$. The application of trapezoidal rule to (13) gives

$$\frac{\Delta\eta}{2}\left(RU_0^{(n)}+U_{(m)}^{(n)}\right)+\Delta\eta\sum_{i=1}^{m-1}U_1^{(n)}(R+i\Delta\eta)=\left(\frac{1-R^2}{\eta}\right) \tag{19}$$

The boundary conditions (14) gives

$$U_0^{(n)}=U_0^{(m)}=0$$

The above equation reduces to

$$\Delta\eta\sum_{i=1}^{m-1}U_1^{(n)}(R+i\Delta\eta)=\left(\frac{1-R^2}{\eta}\right) \tag{20}$$

The set of above equations (15)–(18) and (20) has been solved using an iterative process. At first, (17) has been solved at $n=0$ column, and i has been varied from 1 to m-1 to obtain a system of linear equations which is then solved using the Gauss-Jordan method to obtain tangential velocity. m is the number of radial increments in the numerical mesh network. Correspondingly (16), (18) and (20) have also been solved under similar conditions to determine the system of linear equations. By Gauss-Jordan method, these systems are then solved to obtain the axial velocity and pressure at adjacent column $n=1$. Finally, the radial velocity is obtained from (15) by Gauss-Jordan method using the known values of U. By repeating the above procedure, we get the result column by column along the axial direction of the annulus until the flow is fully developed, both axially and tangentially.

4. Results and discussion: The computations have been done by fixing the Bingham number as 10 for different aspect ratio. The solid volume fraction of the nanofluid considered are 0.5 and 1.5 for both copper and silver nanofluids. Moreover, the ratio between the reference density of the solid fraction and the reference density of the fluid fraction for copper and silver

Table 1 Non-Newtonian flow parameters and different volume fraction parameters in tabular form

Nanofluids	B	ϕ	ρ_s	ρ_f
Cu with water	10	0.5 and 1.5	8933	997.1
Ag with water	10	0.5 and 1.5	10,500	997.1

nanofluids are 8.9590 and 10.5305. We fix the ratio of Reynolds number to Taylors number as 20, 30 and the results have been obtained at radial direction 0.02, 0.03 and axial direction 0.007, 0.002, respectively. The velocity profiles along axial, radial, tangential and pressure distribution along the radial direction have been computed for different aspect ratios are 0.3 and 0.8, when the inner cylinder is rotating and the outer cylinder is at rest (Table 1).

The development of tangential velocity profiles in the entrance region is depicted in Figs. 3 and 4 for the aspect ratio of large annular space ($R = 0.3$) and a small annular space ($R = 0.8$), respectively. Here the volume fraction parameter impacts the tangential velocity much, which is high for a small value. The tangential velocity decreases from the inner cylinder to the outer cylinder in a gradual but linear manner, immaterial of the annular width. For a higher value of volume fraction 1.5, this decreasing pattern is in an oscillation nature in a large annular space for both Bingham nanofluids. However, when space is small, the tangential profile takes the shape of convex form for both silver and copper nanofluids. However, silver nanofluid takes a good development in the tangential velocity rather than copper nanofluid.

Figs. 5 and 6 depict the axial velocity profiles for the same value of volume fraction and aspect ratio taken earlier. It is observed that for a low volume fraction irrespective of annular space, the axial velocity component increases from the inner wall to reach its maximum at a particular radial position and then decreases as it moves towards the outer wall of the annular cylinder. However, for a high volume fraction, the above trend remains the same for the small annular space. However, the above-mentioned trend is oscillating for a large annular space. Further, irrespective of the two nanofluids under consideration, for the low volume fraction, the difference in the values of axial velocity at any radial position between the two cylinders is found to be marginal. Whereas, for high volume fraction, the difference in the values of axial velocity is found to be marginal for the small annular space and difference is significant for a large annular space. Silver nanofluid develops in quick time than copper nanofluid. Therefore we can conclude the length of the entrance region is smaller for a silver nanofluid than that of copper nanofluid. This may be due to their physical properties with flow nature.

The radial velocity, for the above-mentioned aspect ratio and the volume fraction parameters, is presented in Figs. 7 and 8. For any annular space and volume fraction, the radial velocity profile is found to follow sinusoidal behaviour. It has been realised that for silver and copper nanofluids, at any radial position, the difference between the values of the radial velocity is found to be negligible. For high volume fraction, the difference is negligible in the small annular space and significant in large annular space. Silver nanofluid takes high magnitude of radial velocity with the negligible difference between the Bingham nanofluids.

The pressure distribution computed for various cases is shown in Figs. 9 and 10. For all the parameters considered, the pressure increased gradually from inner rotating cylinder to outer stationary cylinder. However, this increase is very small in magnitude for

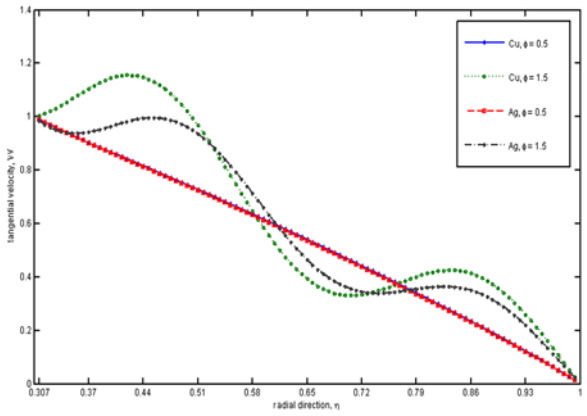

Fig. 3 *Tangential velocity for R = 0.3, Z = 0.02, B = 10 then Ø = 0.5 and 1.5*

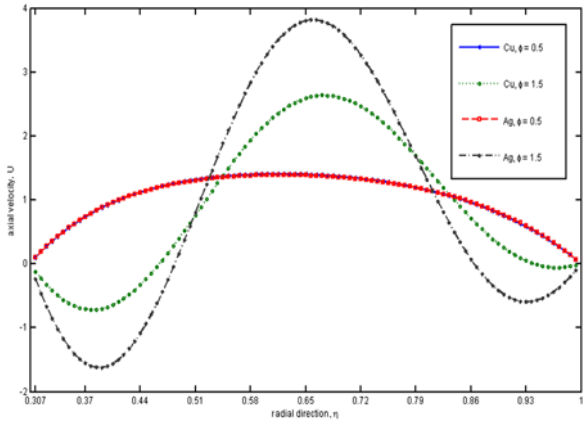

Fig. 5 *Axial velocity for R = 0.3, Z = 0.02, B = 10 then Ø = 0.5 and 1.5*

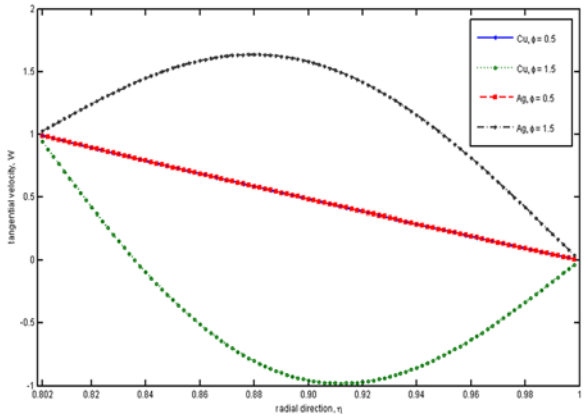

Fig. 4 *Tangential velocity for R = 0.8, Z = 0.02, B = 10 then Ø = 0.5 and 1.5*

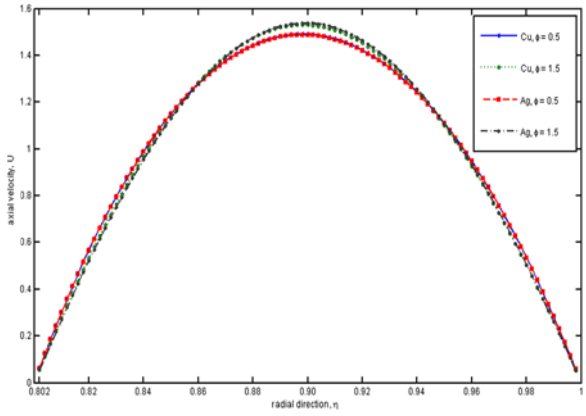

Fig. 6 *Axial velocity R = 0.8, Z = 0.02, B = 10 then Ø = 0.5 and 1.5*

doi: 10.1049/mnl.2019.0437

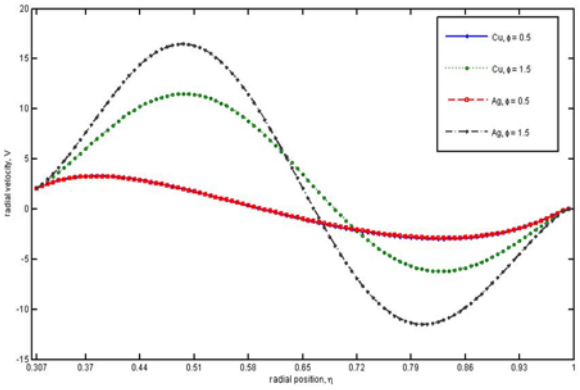

Fig. 7 *Radial velocity for R = 0.3, Z = 0.02, B = 10 then Ø = 0.5 and 1.5*

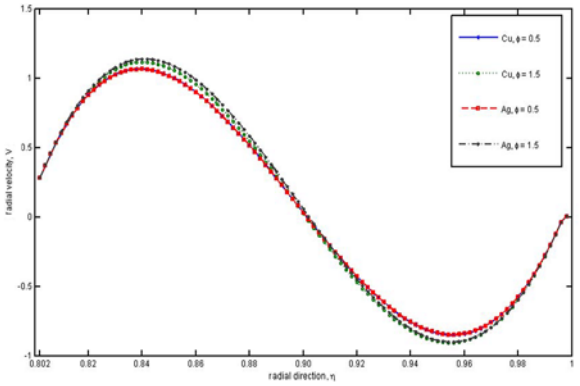

Fig. 8 *Radial velocity for R = 0.8, Z = 0.02, B = 10 then Ø = 0.5 and 1.5*

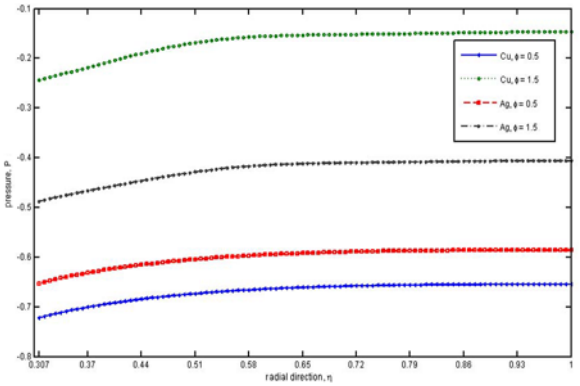

Fig. 9 *Pressure drop for R = 0.3, Z = 0.02, B = 10 then Ø = 0.5 and 1.5*

the narrow space cylinders. Copper nanofluid showed a higher pressure when compared to silver nanofluid irrespective of aspect ratio. It has been observed that the pressure in the annuli is found to be less for the copper nanofluid than that of silver nanofluid provide the volume fraction assumes that value from 0.1 to 1.1. However, this trend is reversed for the volume fraction 1.2–2. Also it has been observed as the volume fraction increase the pressure also increases for both nanofluids. However, the rate of increase is much higher for copper nanofluid than that of silver nanofluid. Bingham nanofluids are inversely proportional to the viscous nature. Silver nanofluid coalescing with Bingham fluid decreases the pressure better than copper nanofluid coaleascing with Bingham fluid in the entrance region of the annuli.

The above-mentioned observations are compared with the results of Nadiminti and Kandasamy [7] in similar conditions, without adding nanoparticles to the Bingham fluid and it has been found

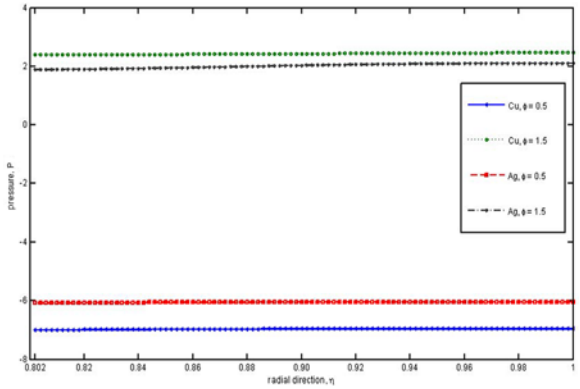

Fig. 10 *Pressure drop for R = 0.8, Z = 0.02, B = 10 then Ø = 0.5 and 1.5*

that our results are in good agreement with the results of above-mentioned authors. The case of stationary concentric annular cylinders, the results of axial velocity components in the analysis matched well with the results of Kandasamy [8].

5. Conclusion: Low volume fraction does not have an impact on velocity profiles (axial, radial and tangential) irrespective of aspect ratio. From Figs. 3–10 for low volume fraction, copper (Cu) and silver(Ag) nanofluids have a similar trend of velocity profiles, which may be because of Newtonian behaviour and for higher volume fractions, Ag-nanofluid showed a higher magnitude compared to copper nanofluid because of its physical properties like density and viscosity. The time taken for the silver nanofluid to flow between the annular cylinders obviously dissipates the heat generated due to friction comparatively better than copper nanofluid. Pressure drop is more for higher volume fraction, because of the viscous nature of nanofluids when compared with base fluid and lower volume fractions of the nanofluids. From Figs. 3–10, a higher volume fraction of copper nanofluid showed a higher pressure drop when compared to silver nanofluids. Higher pressure drop increases the pumping power and cost which is not suitable for practical applications.

6. Acknowledgment: The authors thank the Principal and management of SSN institutions for their support in carrying out this work.

7 References

[1] Choi S.U.S., Eastman J.A.: 'Enhancing thermal conductivity of fluids with nanoparticles'. ASME Int. Mechanical Engineering Congress & Exposition, San Francisco, CA, 12–17, 1995

[2] Chen H., Ding Y., Tan C.: 'Rheological behavior of nanofluids', *New J. Phys.*, 2007, **9**, p. 367

[3] Hojjat M., Etemad S.G., Bagheri R., *ET AL.*: 'Convective heat transfer of non-newtonian nanofluids through a uniformly heated circular tube', *Int. J. Thermal Sci.*, 2011, **50**, pp. 525–531

[4] Esmaeilnejad A., Aminfar H., Neistanak M.s.: 'Numerical investigation of forced convection heat transfer through microchannels with non-Newtonian nanofluids', *Int. J. Thermal Sci.*, 2014, **75**, pp. 76–86

[5] Hayat T., Asad S., Alsaedi A.: 'Flow of Casson fluid with nanoparticles', *Appl. Math. Mech.*, 2016, **37**, (4), pp. 459–470

[6] Usman M., Soomro F.A., Ul Haq R.C., *ET AL.*: 'Thermal and velocity slip effects on casson nanofluid flow over an inclined permeable stretching cylinder via collocation method', *Int. J. Heat Mass Transf.*, 2018, **122**, pp. 1255–1263

[7] Nadiminti S.R., Kandasamy A.: 'Entrance region flow heat transfer in concentric annuli with rotating inner wall for bingham fluid', *J. Comput. Appl. Mech.*, 2016, **11**, (2), pp. 137–157

[8] Kandasamy A.: 'Entrance region flow heat transfer in concentric annuli for a Bingham fluid'. Proc. of Third Asian-Pacific Conf. on Computational Mechanics, Seoul, Korea, 1996, pp. 1697–1702